(Received 25 May 2025, Accepted 21 July 2025, Scheduled 3 August 2025)

Improved Model Predictive Torque Control for PMSM Based on Anti-Stagnation Particle Swarm Online Parameter Identification

Yang Zhang[1], Ping Yang[1], Chenhui Liu[1], Sicheng Li[1], Kun Cao[1], Ziying Liu[1], and Zhun Cheng[2,*]

[1] *Hunan University of Technology, Zhuzhou 412007, China*
[2] *Hunan Railway Professional Technology College, Zhuzhou 412001, China*

ABSTRACT: To address the problem that the control performance of permanent magnet synchronous motor (PMSM) in model predictive torque control (MPTC) is highly sensitive to motor parameters, an improved model predictive torque control scheme for PMSM based on anti-stagnation particle swarm online parameter identification (ASPSO-IMPTC) is proposed. First, an improved MPTC strategy based on inductance and magnetic chain parameter compensation is proposed. Compared with conventional MPTC, the proposed method can acquire accurate motor parameters in real-time, thereby enhancing both the control performance and parameter robustness of PMSM. Second, a review mechanism is proposed to enhance traditional PSO parameter identification. This method prevents particle swarm stagnation, enhances the parameter identification ability of the traditional method, and improves the real-time accuracy of the motor parameters. The parameter robustness of the motor is further enhanced. Finally, the experimental results show that the proposed ASPSO-IMPTC strategy can effectively improve the control performance and parameter robustness of PMSM when parameters mismatch occurs in PMSM.

1. INTRODUCTION

PMSMs are extensively applied in industrial production, aerospace, and other applications due to their high efficiency, compact size, and power density [1]. The control methods primarily include field-oriented control (FOC) and direct torque control (DTC) [2]. The FOC selects voltage vectors based on torque and flux linkage errors using a predefined switching table. While this method is simple, it has limited voltage vector options, leading to significant torque and flux ripple [3]. To mitigate the high flux linkage and torque ripple in DTC, researchers worldwide have introduced model predictive control (MPC) with notable success. MPC, which is widely used in power electronics, can be categorized into continuous control set MPC (CCS-MPC) and finite control set MPC (FCS-MPC) [4]. In the PMSM drive system, FCS-MPC methods can be categorized into model predictive current control (MPCC) and model predictive torque control (MPTC) based on different control objectives [5].

MPTC control performance is closely related to the model parameters, and when real parameters are affected by the temperature rise, magnetic field saturation, and other factors, the torque and magnetic chain prediction will produce errors, which deteriorate the control performance [6, 7]. To address the above problems, scholars have done much research and proposed various solutions.

To address the problem of MPTC performance being heavily dependent on parameters, scholars have done the following research on MPTC itself. In [8], a modified MPCC with a current variation update mechanism is proposed, which can suppress parameter mismatch perturbation, but the improvement is limited. In [9], a simplified stator magnetic chain observer is introduced, offering improved dynamic performance and enhanced parameter robustness compared to the traditional PI-MPTC, though it suffers from high computational complexity. In [10], a motor-parameter-free MPCC is introduced, and it can significantly improve the control performance under motor parameter mismatch, but it is complicated to construct the motor model. In [11], an MPTC based on sliding mode control is introduced. The proposed method has the best immunity and robustness to motor parameter variations and load torque variations, but the control effect depends on the parameter settings. In [12], a robust model predictive voltage control method is proposed. This method effectively enhances the robustness of PMSMs and eliminates the impact of parameter mismatch on motor control performance.

Moreover, in addition to enhancing the robustness of the MPTC strategy to parameter variations within the strategy itself, scholars have conducted the following research from the perspective of parameter identification. In [13], two online recognition schemes based on Kalman filters are proposed. One employs an extended Kalman filter (EKF), while the other uses a double EKF. These schemes are applicable to identifiable parameter combinations, though with limited accuracy. In [14],

* Corresponding author: Zhun Cheng (120277982@qq.com).

an improved deadbeat (DB) predictive current control (DPCC) scheme based on multiparameter identification is proposed. The scheme has effectively solved the problem of indeterminate equations of multiparameter identification. It has the advantages of short convergence time and low identification error, but it has the problem of large computation. In [15], a parameter identification method based on high frequency equivalent resistance models and resistance and flux detection algorithm was proposed for parameter sensitivity analysis. The proposed method has an excellent recognition effect under various operation conditions. In [16], a new algorithm of online parameter identification for PMSM by using differential beatless control is proposed. Firstly, a recognition model is developed to estimate parameter error from the offset of DB control. Then, a new parameter permutation method is proposed to address the rank deficiency problem in the parameter identification process. In [17], a method for parameter identification using an online particle swarm optimization (PSO) to obtain critical PMSM parameters such as magnetic flux and inductance is proposed. The proposed method is effective in reduced harmonic levels and current following errors due to parameter mismatch, but suffers from particle swarm update stagnation.

Regarding the application of PSO algorithms in PMSM parameter identification, extensive research has been conducted. In [18], a global parameter estimation method for PMSM is proposed. This strategy employs a dynamic self-learning PSO algorithm to track electrical, mechanical, and inverter-related parameters of the PMSM. Although it achieves accurate tracking of electrical parameter variations, its parameter design is relatively complex. In [19], an optimization PSO algorithm is proposed that can measure the inductance and resistance of PMSM using experimental measurements but is prone to the stagnation problem. In [20], a contraction factor anti-predation PSO algorithm is proposed to solve the time to death and equation under-rank problems. This method can improve the control performance of PMSM under parameter mismatch, but the parameter design is more complicated. A distance-guided adaptive PSO using normalization was introduced in [21], demonstrating superior robustness and convergence characteristics in electromagnetic inverse problems. Moreover, an online parameter estimation method for PMSM based on PSO with a dynamic inertia weight strategy was reported in [22], which effectively improved convergence speed and identification accuracy. These studies highlight the growing interest in developing advanced PSO variants for real-time motor control applications.

To address the problem that MPTC control performance in PMSM is affected by motor parameters, the ASPSO-IMPTC strategy is proposed. Compared with conventional MPTC (CMPTC), when the motor parameters are changed, the method still enables the motor to obtain better control performance and strong parameter robustness, and the key contributions from this paper are as below:

1) The IMPTC control strategy returns the motor parameters after parameter mismatch to the motor model by using the parameter extraction compensation method. The control performance of PMSM under parameter mismatch is improved.

2) The proposed ASPSO strategy introduces PSO parameter identification with anti-stalling function, which enables it to recognize the identified motor parameters more accurately. The control performance of the motor under parameter mismatch is improved.

The contents of the rest of the paper are organized as follows. Section 2 introduces the basic concepts and mathematical models of CMPTC and PSO algorithms. Section 3 introduces the basic principle of IMPTC based on parameter extraction compensation method. Section 4 shows the basic principle of ASPSO-IMPTC. Section 5 presents experimental verification and simulation analysis. Finally, Section 6 briefly summarizes the paper.

2. THE BASIC CONCEPTS AND MATHEMATICAL MODELS OF THE CMPTC AND PSO

2.1. The Basic Concepts and Mathematical Models of CMPTC

The mathematical model of a surface mounted PMSM in a *dq*-axis rotational coordinate system can be represented as shown below:

$$\begin{cases} u_d = R_s i_d + \frac{d\psi_d}{dt} - \omega_e \psi_q \\ u_q = R_s i_q + \frac{d\psi_q}{dt} + \omega_e \psi_d \end{cases} \tag{1}$$

$$\begin{cases} \psi_d = L_s i_d + \psi_f \\ \psi_q = L_s i_q \end{cases} \tag{2}$$

$$T_e = \frac{3}{2} p \psi_f i_q \tag{3}$$

where u_d and u_q are the *dq*-axis components of stator voltage vector; i_d and i_q are the *dq*-axis components of stator current vector; ψ_d, ψ_q and ψ_f are the *dq*-axis components of stator and rotor magnetic chain vector; R_s and L_s are stator resistance and stator inductance; and ω_e is the rotor angular velocity of the motor. T_e is the electromagnetic torque.

Using the first-order Eulerian discretization method to discretize (1), the following current prediction model is obtained:

$$\begin{cases} i_d(k+1) = \left(1 - \frac{T_s R}{L_s}\right) i_d(k) + T_s \omega_e i_q(k) + \frac{T_s}{L_s} u_d(k) \\ i_q(k+1) = \left(1 - \frac{T_s R}{L_s}\right) i_q(k) - T_s \omega_e i_d(k) + \frac{T_s}{L_s} u_q(k) \\ \qquad\qquad - \frac{T_s \omega_e \psi_f}{L_s} \end{cases} \tag{4}$$

$$T_e(k+1) = \frac{3}{2} p \psi_f i_q(k+1) \tag{5}$$

$$|\psi_s(k+1)| = \sqrt{\left(L_s i_d(k+1) + \psi_f\right)^2 + \left(L_s i_q(k+1)\right)^2} \tag{6}$$

where k represents the sampling value at the current time, $k+1$ the sampling value at the next time, and T_s the value of sampling period.

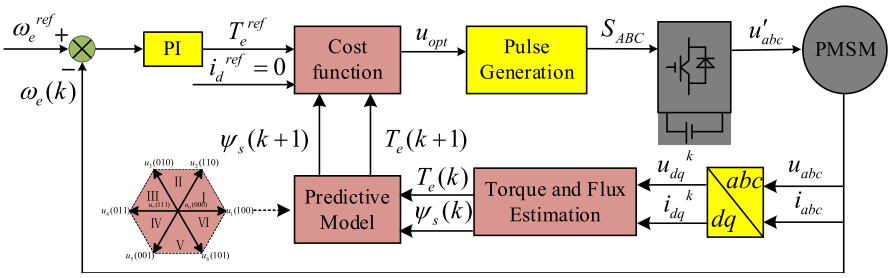

FIGURE 1. The control diagram of CMPTC.

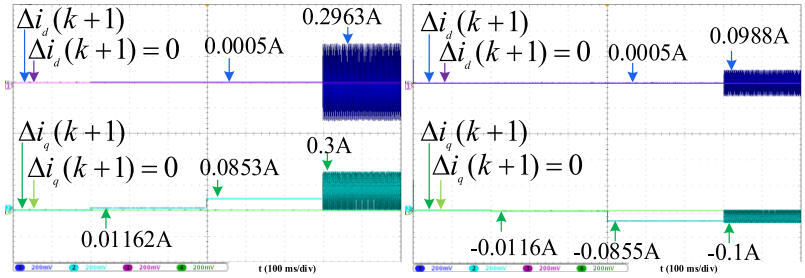

(a) (b)

FIGURE 2. The diagram of current prediction error plot for PMSM parameter mismatch. (a) The parameter mismatch is 50%. (b) The parameter mismatch is 150%.

CMPTC is usually optimized in terms of torque and magnetic chain, thus the cost function is usually set as shown below:

$$g = \left|T_e^{ref} - T_e(k+1)\right| + \lambda \left|\psi_s^{ref} - |\psi_s(k+1)|\right| \tag{7}$$

where λ is a weighting coefficient, which is usually designed using an empirical method; T_e^{ref}, ψ_s^{ref} represent the reference values of torque and magnetic chain.

The control diagram of CMPTC is shown in Fig. 1. The major steps of CMPTC include selecting voltage vectors, designing the cost function, and selecting the optimal voltage vectors. The processes are as follows: first, the seven fundamental voltage vectors (six effective voltage vectors and one zero vector) generated by the inverter are brought into current prediction model (4), which yields the predicted value of each fundamental voltage vector after one sample period. Then, the vectors are input into (7), and the voltage vector that minimizes the cost function is selected as the optimal voltage vector. Finally, the switching state corresponding to the optimal voltage vector is applied to the inverter, which in turn generates the desired three-phase current to control the PMSM.

2.2. The Parametric Sensitivity Analysis of CMPTC

From (5) and (6), it is clear that the accuracy of torque and magnetic flux prediction at the next time step is strongly dependent on the accuracy of the PMSM parameters. When the motor temperature increases, or other harsh operating conditions occur, the motor parameters will change, which in turn makes the original motor model inaccurate and leads to deviations in the predicted values. Therefore, it is essential to investigate the parameter sensitivity in MPTC.

From (4), it can be seen that the current prediction model after occurrence of parameter mismatch is shown below:

$$\begin{cases} i_d^w(k+1) = \left(1 - \frac{T_s(R+\Delta R)}{L_s+\Delta L_s}\right) i_d(k) + T_s\omega_e i_q(k) \\ \qquad + \frac{T_s}{L_s+\Delta L_s} u_d(k) \\ i_q^w(k+1) = \left(1 - \frac{T_s(R+\Delta R)}{L_s+\Delta L_s}\right) i_q(k) - T_s\omega_e i_d(k) \\ \qquad + \frac{T_s}{L_s+\Delta L_s} u_q(k) - \frac{T_s\omega_e(\psi_f+\Delta\psi_f)}{L_s+\Delta L_s} \end{cases} \tag{8}$$

where ΔR, ΔL_s, $\Delta\psi_f$ represent the error between actual and true values of resistance, inductance, and magnetic chain; $i_d^w(k+1)$ and $i_q^w(k+1)$ represent predicted values of dq-axis currents after parameter adaptation occurs.

According to (4) and (8), the current prediction error, caused by parameter mismatch, can be expressed as:

$$\begin{cases} \Delta i_d(k+1) = i_d^w(k+1) - i_d(k+1) \\ = \frac{T_s[(R\Delta L_s - \Delta R L_s) i_d(k) - \Delta L_s u_d(k)]}{L_s(L_s+\Delta L_s)} \\ \Delta i_q(k+1) = i_q^w(k+1) - i_q(k+1) \\ = \frac{T_s[(R\Delta L_s - \Delta R L_s) i_q(k) - \Delta L_s u_q(k) + \omega_e(\psi_f \Delta L_s - \Delta\psi_f L_s)]}{L_s(L_s+\Delta L_s)} \end{cases} \tag{9}$$

where $\Delta i_d(k+1)$ and $\Delta i_q(k+1)$ represent the prediction error of dq-axis current when parameter mismatch occurs.

To verify the degree of influence on the prediction error of model parameters, we conducted the following mismatch condition experiments: the resistance mismatch occurs at 0.2; the magnetic chain mismatch occurs at 0.5 s; the inductance mismatch occurs at 0.8 s. Fig. 2(a) shows the case of 50% parame-

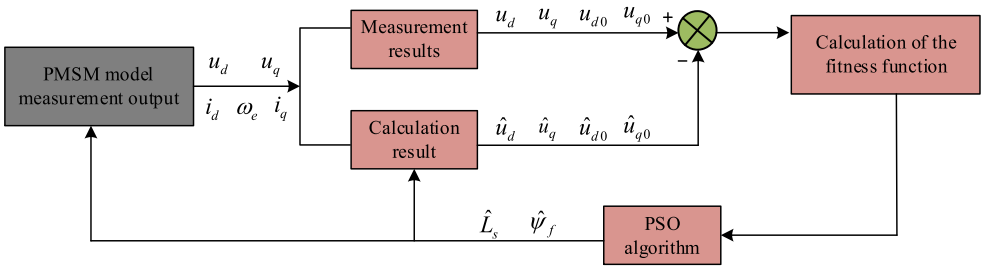

FIGURE 3. The control diagram of PMSM parameter identification based on PSO algorithm.

ter mismatch, and Fig. 2(b) shows the case of 150% parameter mismatch.

As can be seen, the parameter mismatch between inductance and magnetic chain has a significant impact on the forecast error, and resistance mismatch has a smaller effect on prediction error. This is because, during resistance mismatch, its amplification effect is considered nearly constant due to the short control period, resulting in minimal prediction error variation. When the mismatch occurs in the magnetic chain, the q-axis current prediction error increases. Inductance mismatch leads to increased prediction errors in both d-axis and q-axis currents. Prediction errors are eliminated only when the PMSM parameters are accurate, allowing the motor to operate with improved control performance.

Thus, to avoid the degradation of motor control performance due to parameter mismatch, this paper starts from the IMPTC based on parameter extraction and compensation and online parameter identification to carry out the system parameter robustness study.

2.3. The Basic Concepts and Mathematical Models of PSO

The basic principle of parameter identification is as follows. Firstly, the actual model is compared with the theoretical model. Subsequently, a fitness function is computed, and the result is passed to the intelligent optimization algorithm Finally, the intelligent algorithm optimizes the identified values in the theoretical model to make them close to the real values.

There are many approaches to parameter identification [23–25], such as Genetic Algorithms (GA), Neural Networks (NN), and extended Kalman filter (EKF) algorithms. GA global search is powerful but computationally intensive. NN is adaptable but requires a significant amount of training data. EKF is commonly used to deal with nonlinear problems, but the parameter design is complex. However, PSO algorithm is simple to implement and has fast convergence speed, so this paper investigates how to enhance parameter identification performance of motor from the point of view of PSO.

The PSO algorithm is a stochastic optimization algorithm based on population intelligence, in which each individual is a particle that represents a reasonable solution. It updates individual optimal results and global optimal results of the particles by continuously adjusting the position and speed of the particles until the objective function is satisfied, and a global optimal solution position is found. The iterative optimization formula of PSO is shown as follows:

$$\begin{cases} v_i^{k+1} = wv_i^k + c_1 rand_1 \times \left(p_{best} - x_i^k\right) \\ \qquad\quad +c_2 rand_2 \times \left(g_{best} - x_i^k\right) \\ x_i^{k+1} = x_i^k + v_i^{k+1} \end{cases} \tag{10}$$

where v_i denotes the iteration speed of the particle; x_i represents the position of the particle; k is the number of iterations; w is inertia weight; c_1 and c_2 are the learning factors; p_{best} is the local optimal solution; and g_{best} is the global optimal solution.

The PSO algorithm parameter identification needs to identify the parameters of four parameter values. In this paper, the PMSM is a hidden pole machine, in addition to that the change of resistance of the motor control performance has less impact, so only needs to identify stator magnetic chain and stator inductance.

The principle of PMSM parameter identification based on PSO algorithm is shown in Fig. 3. u_d, u_q, u_{d0}, and u_{q0} are the measured outputs of the actual model; $\hat{u}_d$, $\hat{u}_q$, $\hat{u}_{d0}$, and $\hat{u}_{q0}$ are the outputs of the adjustable model; $\hat{L}_s$ and $\hat{\psi}_f$ are the recognized result values.

3. THE BASIC PRINCIPLE OF IMPTC

In order to reduce the impact of parameter mismatching on the MPTC control performance, this section presents an IMPTC based on the parameter extraction compensation method from the traditional MPTC control principle. The control diagram is shown in Fig. 4.

When the resistance is mismatched, (9) becomes (11), and it can be seen that the order of magnitude of T_s/L_s is too small to consider the effect of the resistor mismatch [26]. Moreover, the conclusion is used in the proposed methodology.

$$\begin{cases} \Delta i_d(k+1) = \frac{-T_s \Delta R i_d(k)}{L_s} \\ \Delta i_q(k+1) = \frac{-T_s \Delta R i_q(k)}{L_s} \end{cases} \tag{11}$$

In this paper, we focus on extracting inductance and magnetic chain information from the dq-axis current prediction error to compensate for inaccuracies in inductance and magnetic chain parameters caused by parameter mismatch. This approach enhances the parameter robustness of MPTC and improves motor control performance.

Since the impact of resistive mismatch on the current prediction error is very small, this segment only focuses on extraction

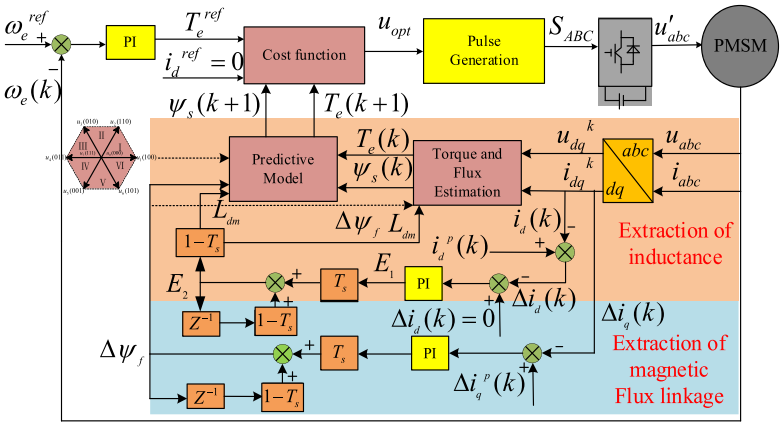

FIGURE 4. The control diagram of IMPTC.

methods for inductance and magnetic chains. After neglecting the effect of resistive mismatch, the equation of d-axis current prediction error is as follows:

$$\Delta i_d(k+1) = \frac{T_s \Delta L_s \left[R i_d(k) - u_d(k)\right]}{L_s(L_s + \Delta L_s)} \tag{12}$$

3.1. The Basic Principle of the Inductance Extraction Compensation Method

From (12), d-axis current prediction error contains only inductive information without magnetic chain information, which is consistent with the conclusion that d-axis current error in the parameter sensitivity analysis is affected by the inductive mismatch but not by the magnetic chain mismatch. Therefore, this paper extracts the inductor parameter information from d-axis current prediction error equation, and the control diagram is shown in Fig. 5.

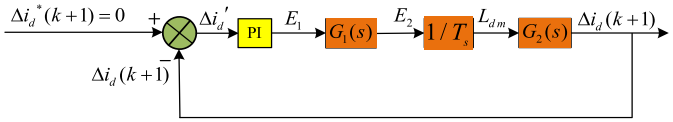

FIGURE 5. The diagram of the extracted inductance.

From Forward Euler Theorem, the expression for output E_1 of proportional-integral (PI) controller in Fig. 5 is shown below:

$$E_1(k) = E_1(k-1) + T_s k_2 \Delta i_d' \tag{13}$$

where $E_1(k)$ represents the inductors information at moment k; $E_1(k-1)$ represents the inductance information at moment $k-1$; $\Delta i_d'$ represents the d-axis current prediction error difference ($\Delta i_d' = \Delta i_d^*(k+1) - \Delta i_d(k+1)$); k_2 represents the PI controller scaling factor.

$G_1(s)$ represents the transfer function of the low-pass filter, and its output transfer function relation is as follows:

$$\begin{cases} E_2(k) - E_2(k-1) = T_s(E_1 - E_2(k-1)) \\ \frac{dE_2(t)}{dt} + E_2(t) = E_1 \\ G_1(s) = \frac{E_2}{E_1} = \frac{1}{s+1} \end{cases} \tag{14}$$

where $E_2(k)$ and $E_2(k-1)$ represent the inductors information acquired at time k and $k-1$. The output of PI controller is E_1.

From (14), the information about the inductance correlation is expressed as in (15).

$$\begin{cases} E_2 = T_s\left(\frac{1}{L_s} - \frac{1}{1+\Delta L_s}\right) \\ L_{dm} = \frac{E_2}{T_s} = \frac{1}{L_s} - \frac{1}{1+\Delta L_s} \end{cases} \tag{15}$$

where L_{dm} represents the information about the inductance, which is used in the compensation with the actual motor model.

By (14) and (15), the transfer function of $G_2(s)$ is expressed as follows:

$$G_2(s) = \frac{\Delta i_d(k+1)}{L_{dm}} = T_s\left[R i_d(k) - u_d(k)\right] \tag{16}$$

In this paper, Maximum Torque Per Ampere is adopted for PMSM, which is the $id = 0$ control for the hidden pole machine, so (16) can be simplified as follows:

$$G_2(s) = -T_s u_d(k) \tag{17}$$

Combining (16) with (17), $G_2(s)$ is simplified as follows:

$$G_2(s) = T_s \omega_e (L_s + \Delta L_s) i_q(k) \tag{18}$$

So the transfer function of the PI controller is shown as follows:

$$G_{PI}(s) = \frac{E_1}{\Delta i_d'} = \frac{k_3}{s} \tag{19}$$

where k_3 represents the scaling factor of the PI controller.

Combining (14), (18) and (19), the open-loop transfer function shown in the schematic block diagram of the inductor extraction compensation method is expressed as follows:

$$\begin{aligned} G(s) &= \frac{G_{PI}(s)G_1(s)G_2(s)}{T_s} = \frac{k\omega_e(L_s + \Delta L_s) i_q(k)}{s(s+1)} \\ &= \frac{k_3 \omega_e L i_q}{s(s+1)} \end{aligned} \tag{20}$$

where L represents the actual inductance value.

Replace the feedback link in Fig. 5 by $H(s)$ with a gain of 1. Therefore, the transfer function of the closed-loop system is as shown below:

$$G_c(s) = \frac{G(s)}{1 + G(s)H(s)} \tag{21}$$

With (21), the gain of the open-loop system is expressed as follows:

$$k_o = k_3 \omega_e L i_q \tag{22}$$

The closed loop characteristic equation based on inductors extraction compensation method can be expressed as below:

$$s^2 + s + k_o = 0 \tag{23}$$

where s represents the field of complex numbers, and k represents the open-loop gain of (21).

The characteristic equation of the second order system can be expressed as follows:

$$s^2 + \xi \omega_n s + \omega_n^2 = 0 \tag{24}$$

where ω_n represents the angular frequency of oscillation of the system, and ξ represents the damping coefficient of PMSM.

To obtain the best response characteristics, the damping ratio $\xi = 0.707$ combined with (23) and (24) yields the relation as follows:

$$\begin{cases} \omega_n = \frac{1}{2\xi} = \frac{\sqrt{2}}{2} = 0.707 \\ k_o = \omega_n^2 = 0.5 \end{cases} \tag{25}$$

From the association of (21) and (23), the expression for the gain k of PI controller is calculated as follows:

$$k_3 = \frac{1}{2\left[\omega_e (L_s + \Delta L_s) i_q(k)\right]} \tag{26}$$

As a result, the appropriate scaling factor can be calculated on-line according to (26), and on this basis, the accurate inductors information L_{dm} can be obtained. From (16), the relationship between L_{dm} and inductance error is shown as follows:

$$\Delta L_s = \frac{L_s(1 + L_{dm}) - 1}{1 - L_s L_{dm}} \tag{27}$$

Taking (27) into current prediction model, due to elimination of the inductance error resulting from the inductance mismatch, the expression for the q-axis current prediction error can be simplified as in (28), where the magnetic chain error is only included in q-axis current error.

$$\Delta i_q(k+1) = \frac{-\Delta\psi_f T_s \omega_e}{L_s + \Delta L_s} \tag{28}$$

3.2. The Basic Principle of the Magnetic Chain Extraction Compensation Method

By referring to the inductive extraction compensation method, the magnetic chain extraction compensation method is as shown in Fig. 6.

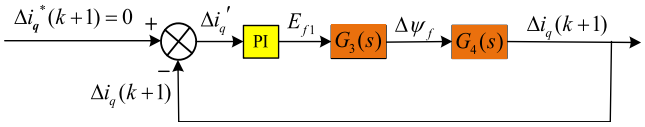

FIGURE 6. The diagram of the extracted magnetic chain.

The magnetic chain error is related to q-axis current prediction error by a transfer function that can be expressed as follows:

$$G_4(s) = \frac{\Delta i_q(k+1)}{\Delta\psi_f} = \frac{-T_s\omega_e}{L_s + \Delta L_s} \tag{29}$$

The control function for extracting the magnetic chain information is designed as follows:

$$\Delta\psi_f(k) = \Delta\psi_f(k-1)(1 - T_s) + E_{f1} \cdot T_s \tag{30}$$

where $\Delta\psi_f(k)$ and $\Delta\psi_f(k-1)$ represent the chain error information obtained at k and $k-1$ moments, and E_{f1} represents the output value of q-axis current prediction error by PI controller.

The application of Laplace transforms to (30) can lead to the following relation.

$$\begin{cases} \frac{d\Delta\psi_f(t)}{dt} + \Delta\psi_f(t) = E_{f1} \\ G_3(s) = \frac{\Delta\psi_f}{E_{f1}} = \frac{1}{s+1} \end{cases} \tag{31}$$

According to (29) and (31), open-loop transfer function of magnetic chain extraction compensation method can be expressed as follows:

$$\begin{aligned} G_{\psi O}(s) &= \frac{-T_s\omega_e}{L_s + \Delta L_s} \cdot \frac{G_{PI}(s)}{s+1} \\ &= \frac{-T_s\omega_e}{L_s + \Delta L_s}\left(K_p + \frac{K_i}{s}\right) \end{aligned} \tag{32}$$

In (32), in order to make the magnetic chain extraction algorithm to obtain better results, it is necessary to require the ratio and integral values to be more accurate. Therefore, closed-loop equation of flux chain extraction compensation method is designed as follows:

$$\begin{cases} s^2 + s + K_2 x_2 s + K_2 = 0 \\ x_2 = \frac{K_p}{K_i} \\ K_2 = K_i \frac{T_s\omega_e}{L_s + \Delta L_s} \end{cases} \tag{33}$$

The normal characteristic equation for a second-order system is presented in (23), and the following relationship can be obtained by combining (32) and (23).

$$\begin{cases} \zeta\omega_n = 1 + K_2 x_2 \\ K_2 = \omega_n^2 \end{cases} \tag{34}$$

By setting the damping coefficient to 0.707, (34) can be rewritten as follows:

$$x_2 K_2 - \zeta\sqrt{K_2} + 1 = 0 \tag{35}$$

The magnetic chain extraction compensation method is similar to the inductor extraction compensation method, and the proportional and integral design of PI controller is as follows:

$$\begin{cases} K_i = \frac{K_2(L_s+\Delta L_s)}{T_s\omega_e} \\ K_p = x_2 K_i \end{cases} \tag{36}$$

where K_2 is set to 0.96, and x_2 is 0.4.

In this section, the proposed IMPTC based on the parameter extraction compensation method can reasonably return the changed motor parameters to the motor when PMSM parameters are changed, which improves the control performance of motor as well as enhances the parameter robustness of the motor. However, the effect of improving the parameter robustness of motor only by model prediction is limited, so Section 3 improves parameter robustness of PMSM further from the viewpoint of parameter identification.

4. THE BASIC PRINCIPLE OF ASPSO-IMPTC

The traditional PSO (TPSO) is an algorithm that searches for optimal solutions offline. Because TPSO is an offline algorithm, it is not well adapted to the dynamic operation of the motor and has some limitations. The optimal fit of the ASPSO-based online PSO parameter identification is not a minimum, but a function of time with respect to the optimal fit, which makes it possible to avoid the occurrence of particle stall updating situation. It is more suitable for the stable operation of motor.

To evaluate the quality of each particle in the online identification process, a fitness function is designed based on the current prediction error. Specifically, both d-axis and q-axis current deviations are calculated at each sampling step, and the fitness function is defined as:

$$f = \rho\,|\Delta id(k+1)| \cdot |\Delta iq(k+1)| \tag{37}$$

where ρ is a positive amplification coefficient.

The reason for choosing this multiplicative form is to ensure that both flux linkage and stator inductance errors contribute to the fitness evaluation. Since q-axis prediction deviation is more sensitive to flux mismatch, while d-axis deviation reflects inductance mismatch, the product of their absolute errors allows the PSO algorithm to simultaneously account for both parameters. This design improves the convergence accuracy and avoids the algorithm falling into local optima that only correct a single parameter.

In online PSO, iteration period is reduced from nT_s to T_s. Reducing computational burden and speeding up convergence is accompanied by some problems of increasing the probability of Type II errors such as undetected and incorrect detection of parameters, for which a new conceptual survey is introduced. The TPSO is a survey each time the adaptation is computed. In online PSO, a survey is needed only when a sampling period is less than a predefined threshold, and each survey implies a kind of update of p_{best} and g_{best}. The ASPSO formula for each survey is as follows:

$$\begin{cases} F_{inv} = \mu_1 f_{av} + \mu_2 f_{\max} \\ \mu_1 + \mu_2 = 1 \end{cases} \tag{38}$$

where f_{av} and $f_{\max}$ represent the average and maximum adaptations of the survey; μ_1 and μ_2 represent the weights of the adaptations.

There are two key parameters p_{best} and g_{best} in the particle swarm algorithm, which represent the optimization direction of all particles. To make sure that all of them select the appropriate g_{best}, a new elimination algorithm is proposed. Only if g_{best} accepts the function's censorship will it be made to remain as a new g_{best}. If the g_{best} is more adaptable than the p_{best} in a review, then the p_{best} is retained as the new g_{best}.

In TPSO, the weight of inertia w impacts convergence speed of particles, and an appropriate increase in its value can improve the global search capability of the particle swarm, while a decrease in its value can enhance the local search capability of the swarm. If w is kept constant throughout optimization process, optimization ability of the TPSO is limited, and it is generally designed as a function that varies with respect to time as a means of allowing the PSO to obtain a faster rate of convergence. When the particle's adaptability is higher, it will make the particle's movement update faster and can find the optimal range faster. So, the optimization iteration about the particle

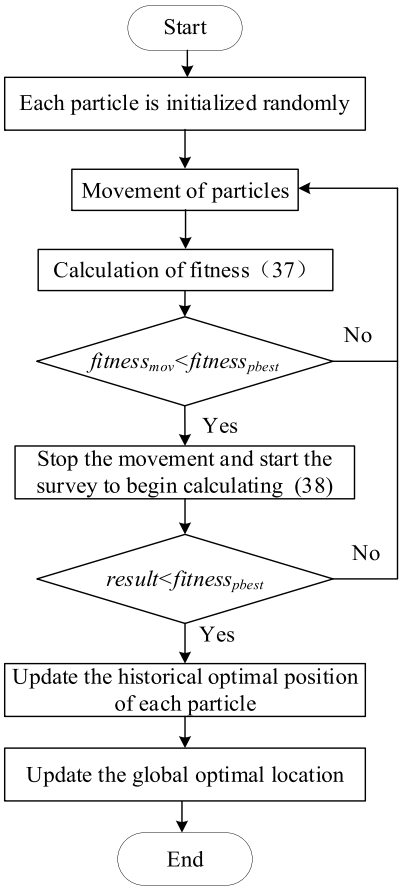

FIGURE 7. The flowchart of the ASPSO strategy.

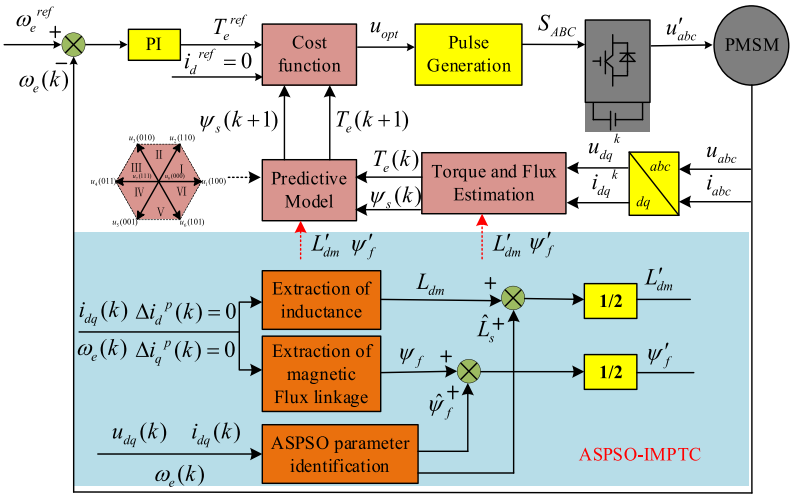

FIGURE 8. The control diagram of ASPSO-IMPTC.

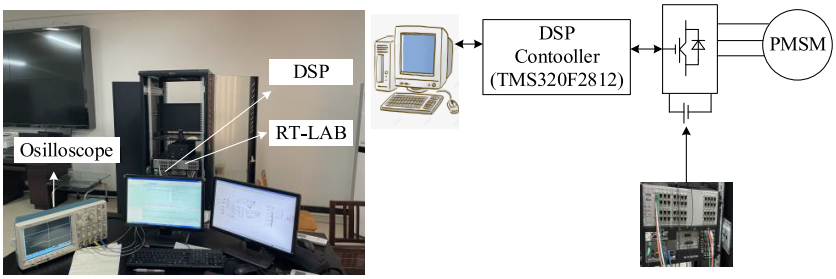

(a) (b)

FIGURE 9. (a) The semi-physical simulation platform. (b) The schematic of RT-LAB hardware-in-the-loop.

swarm can be modified even more as follows:

$$v_i^{k+1} = F_{inv} w v_i^k + c_1 rand_1 \times \left(p_{best} - x_i^k\right) + c_2 rand_2 \times \left(g_{best} - x_i^k\right) \quad (39)$$

Figure 7 shows the flowchart of the program of the ASPSO, which contains two parts: particle updating and reviewing. The review function makes the particle updating of PSO more accurate and rapid and avoids the occurrence of particle stagnation. Compared with the TPSO, the convergence speed and identification accuracy of ASPSO are significantly improved, thus the motor is modeled more accurately, and control performance and parameter robustness of the system are further enhanced.

Combining IMPTC and ASPSO methods, the ASPSO-IMPTC control diagram is shown in Fig. 8. The motor parameters returned by IMPTC and those recognized by ASPSO are averaged and compensated to PMSM in real time. When a parameter mismatch occurs in the motor, ASPSO-IMPTC is able to obtain an accurate motor model in real time, which improves the control performance and parameter robustness of PMSM.

5. EXPERIMENTAL RESULTS AND ANALYSIS

To verify correctness and effectiveness of ASPSO-IMPTC method, the experimental validation is executed on an RT-LAB semi-physical simulation platform with a TMS320F2812 controller. Firstly, the model is downloaded to the simulation platform to realize hardware-in-the-loop system of PMSM system, and then experiment results are displayed through the DPO4034. The sampling frequency of the experimental system is 10 kHz, corresponding to a control loop period of 100 μs. Fig. 9(a) shows the semi-physical simulation platform. Fig. 9(b) shows the schematic diagram of RT-LAB hardware-in-the-loop, and the parameters of PMSM are shown in Table 1. The control parameters of ASPSO-IMPTC are expressed in Table 2.

TABLE 1. The parameters of PMSM.

Parameter	Symbol	Value
Number of pole pairs	n_p	4
Stator inductance	L_s	8.5 mH
Stator resistance	R_s	2.875 Ω
Magnet chain	ψ_f	0.3 Wb
DC voltage	U_{dc}	380 V
Rated torque	T_e	12 N·m
Rated speed	N	1000 r/min
Rated power	P_N	1 kW
Inertia	J	0.00816 kg·m^2

To ensure that the control performance is not affected by immature identification results, the proposed control strategy adopts a buffering mechanism for parameter updating. Specifically, the controller does not immediately apply the identified

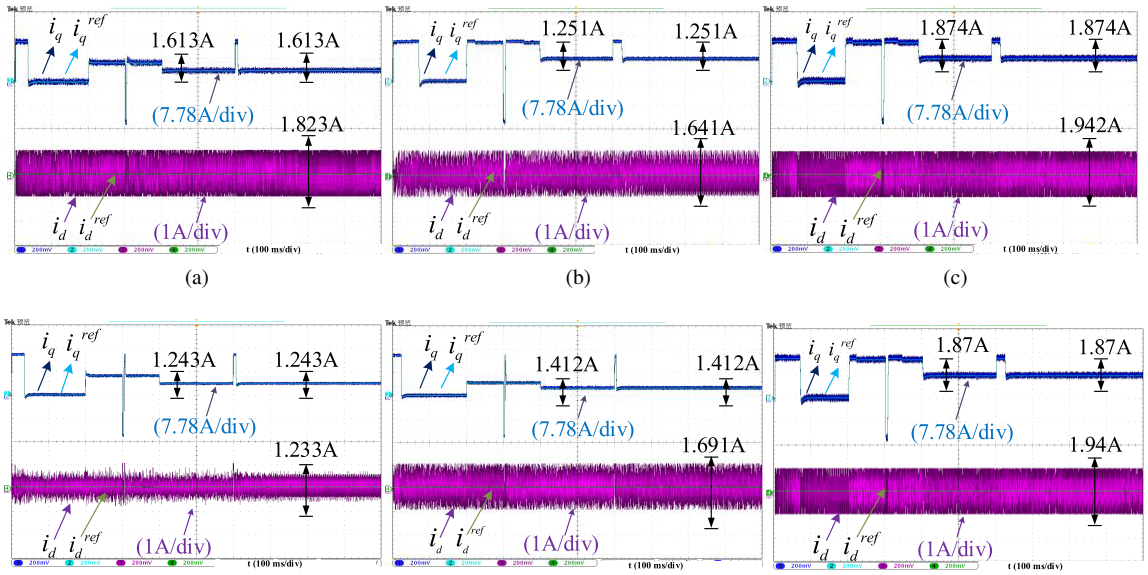

FIGURE 10. The waveform of *dq*-axis current under CMPTC with parameter mismatch. (a) $0.5L_s$, (b) $0.5\psi_f$, (c) $0.5L_s$, $0.5\psi_f$, (d) $1.5L_s$, (e) $1.5\psi_f$, (f) $1.5L_s$, $1.5\psi_f$.

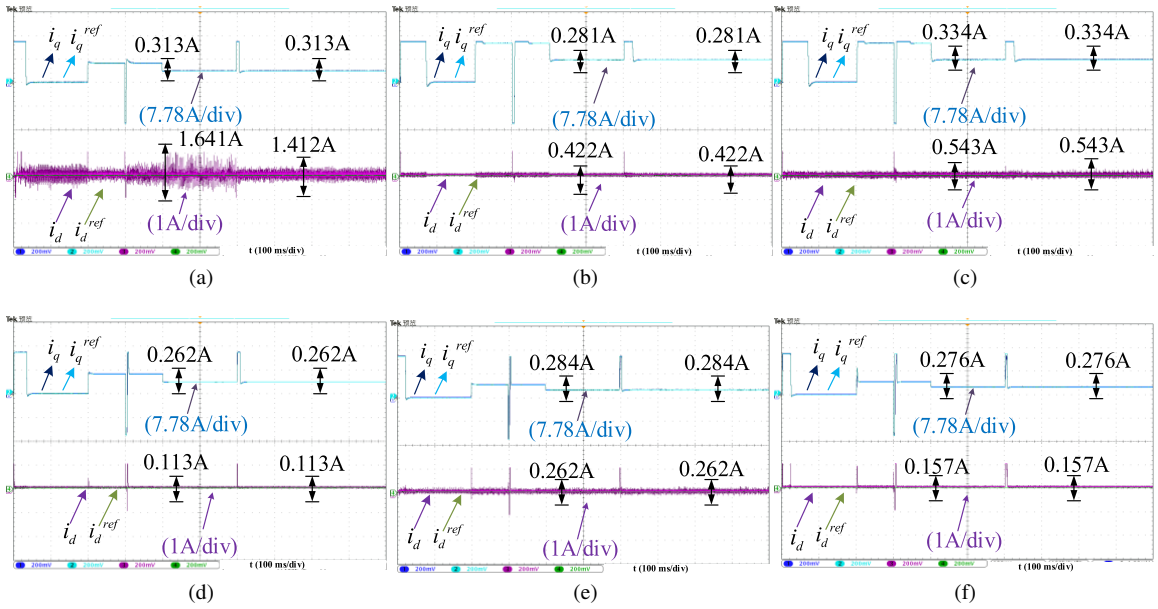

FIGURE 11. The waveform of *dq*-axis current under IMPTC with parameter mismatch. (a) $0.5L_s$, (b) $0.5\psi_f$, (c) $0.5L_s$, $0.5\psi_f$, (d) $1.5L_s$, (e) $1.5\psi_f$, (f) $1.5L_s$, $1.5\psi_f$.

TABLE 2. The control parameters of ASPSO-IMPTC.

Parameter	Value	Description	Source
w	0.6	Inertia weight of PSO	[16]+ tuning
c_1, c_2	2.0	Learning factors	[16]
ρ	1.5	Fitness correction factor	proposed
λ	1/0.05	MPTC cost function weight	tuning

parameters from ASPSO during the initial iterations. Instead, the parameters are updated only when the global best position remains stable for a predefined number of sampling periods. In our implementation, the threshold is set to 3000 sampling periods (i.e., 0.15 s). This approach ensures that the identified parameters are sufficiently close to the actual values before being applied to the control model, thereby avoiding system performance degradation due to premature or inaccurate updates.

The motor operating conditions are arranged as follows: the motor was started at 1000 r/min; the speed decreased to 750 r/min in 0.3 s; and the motor speed increased to 1000 r/min in 0.6 s. The motor starts with no load, runs with a load of 12 N·m in 0.2 s, and the motor load is reduced to 5 N·m in 0.4 s.

The types of parameter mismatches are as follows: the inductance and magnetic chain are simultaneously mismatched by 50% and 150%, respectively.

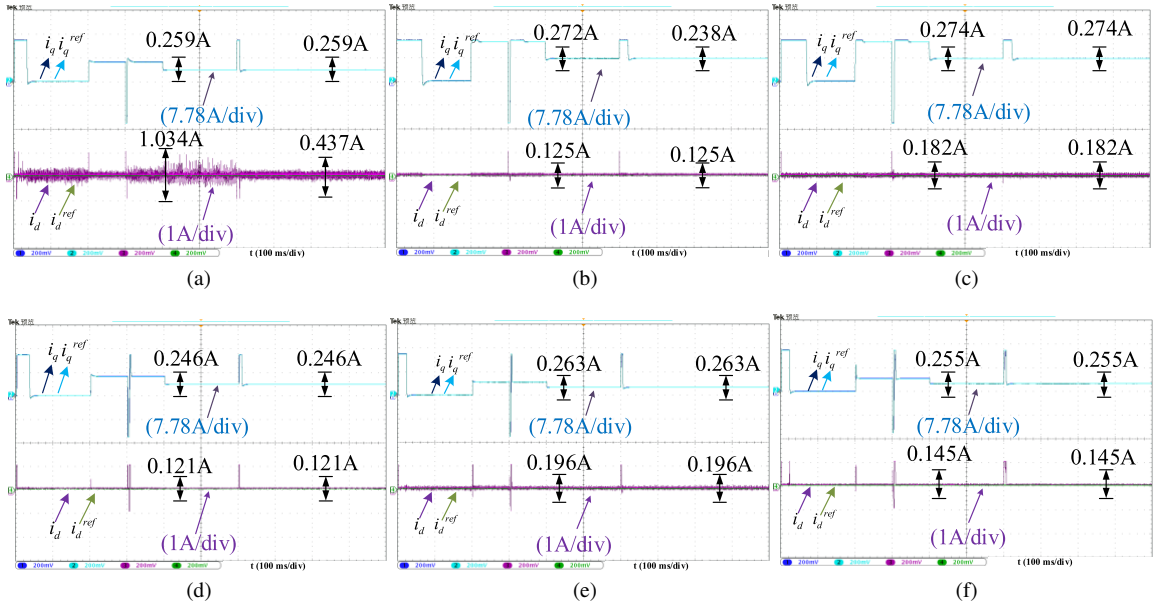

FIGURE 12. The waveform of *dq*-axis current under ASPSO-IMPTC with parameter mismatch. (a) $0.5L_s$, (b) $0.5\psi_f$, (c) $0.5L_s$, $0.5\psi_f$, (d) $1.5L_s$, (e) $1.5\psi_f$, (f) $1.5L_s$, $1.5\psi_f$.

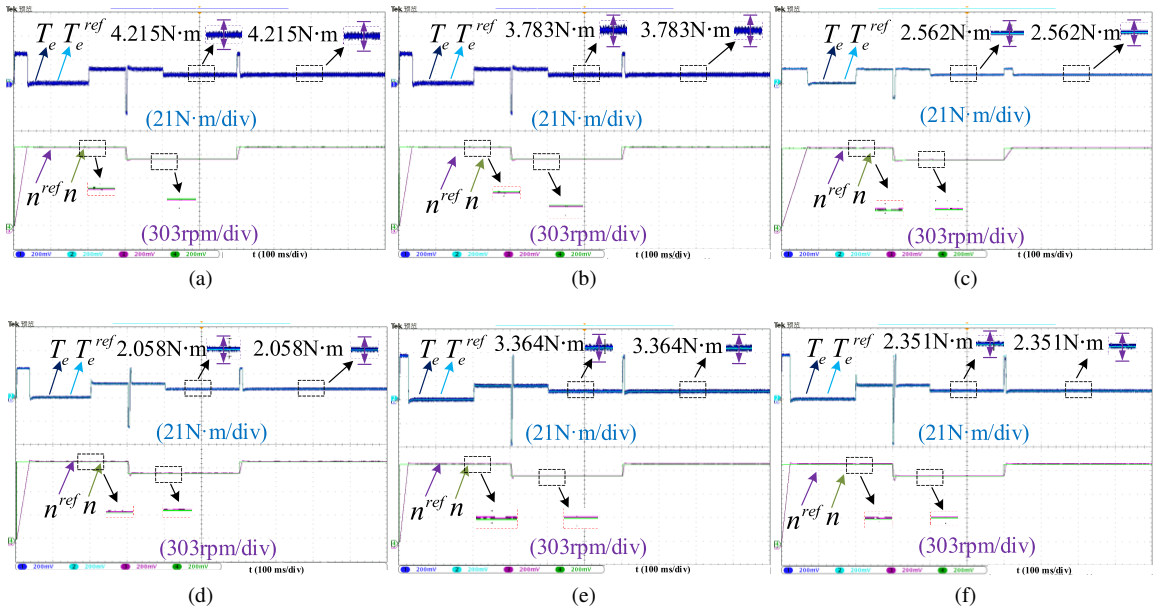

FIGURE 13. The speed and torque waveforms of CMPTC with parameter mismatch. (a) $0.5L_s$, (b) $0.5\psi_f$, (c) $0.5L_s$, $0.5\psi_f$, (d) $1.5L_s$, (e) $1.5\psi_f$, (f) $1.5L_s$, $1.5\psi_f$.

TABLE 3. The pulsation amplitude of the *dq*-axis current.

The type of parameter mismatch	CMPTC		IMPTC		ASPSO-IMPTC	
	i_q (A)	i_d (A)	i_q (A)	i_d (A)	i_q (A)	i_d (A)
$0.5L_s$	1.613	1.823	0.313	1.527	0.259	0.736
$0.5\psi_f$	1.251	1.641	0.281	0.422	0.255	0.125
$0.5L_s$, $0.5\psi_f$	1.874	1.942	0.334	0.543	0.274	0.182
$1.5L_s$	1.243	1.233	0.262	0.113	0.246	0.121
$1.5\psi_f$	1.412	1.691	0.284	0.262	0.263	0.196
$1.5L_s$, $1.5\psi_f$	1.323	1.534	0.276	0.157	0.255	0.145

TABLE 4. The response time and torque pulsation value of the motor speed.

The type of parameter mismatch	CMPTC		IMPTC		ASPSO-IMPTC	
	Respondence time (s)	Torque pulsation value (N·m)	Respondence time (s)	Torque pulsation value (N·m)	Respondence time (s)	Torque pulsation value (N·m)
$0.5L_s$	0.0635	4.215	0.0583	1.265	0.0532	1.137
$0.5\psi_f$	0.0733	3.783	0.0637	0.967	0.00598	0.847
$0.5L_s$, $0.5\psi_f$	0.0692	2.562	0.0592	0.867	0.0543	0.791
$1.5L_s$	0.0627	2.058	0.0576	0.785	0.529	0.785
$1.5\psi_f$	0.0689	3.364	0.0591	0.915	0.0537	0.817
$1.5L_s$, $1.5\psi_f$	0.0618	2.351	0.0563	0.846	0.0531	0.793

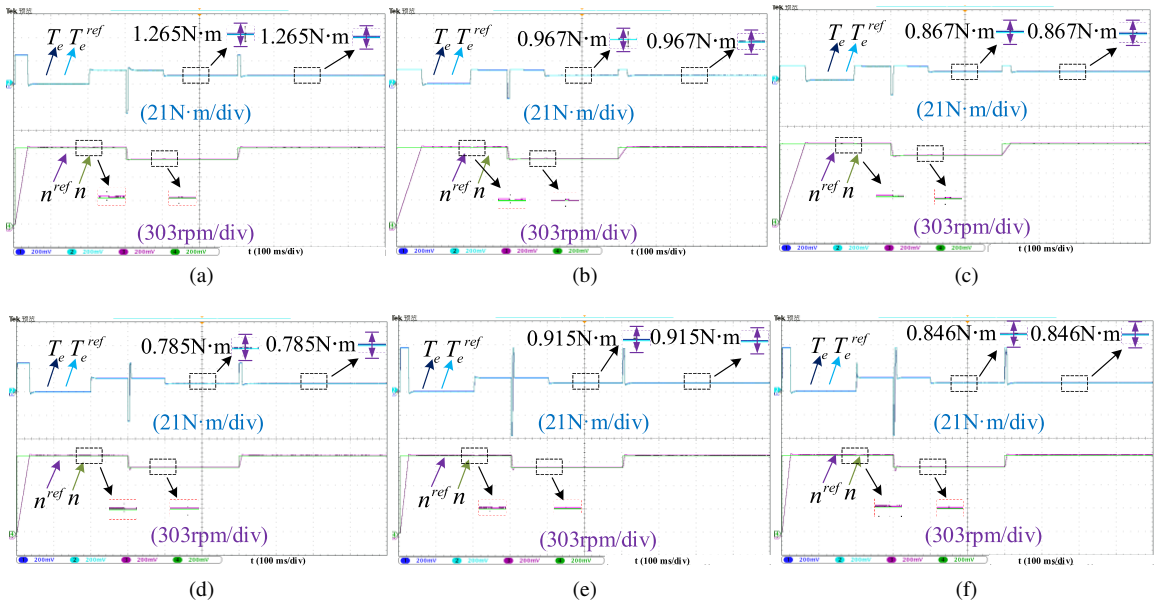

FIGURE 14. The speed and torque waveforms of IMPTC with parameter mismatch. (a) $0.5L_s$, (b) $0.5\psi_f$, (c) $0.5L_s$, $0.5\psi_f$, (d) $1.5L_s$, (e) $1.5\psi_f$, (f) $1.5L_s$, $1.5\psi_f$.

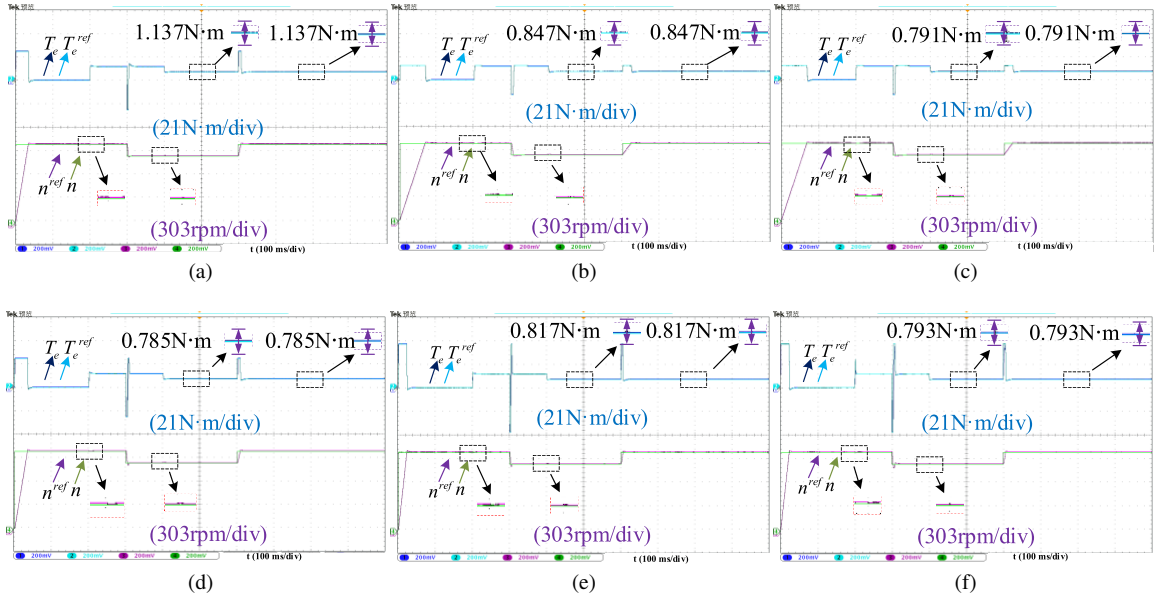

FIGURE 15. The speed and torque waveforms of ASPSO-IMPTC with parameter mismatch. (a) $0.5L_s$, (b) $0.5\psi_f$, (c) $0.5L_s$, $0.5\psi_f$, (d) $1.5L_s$, (e) $1.5\psi_f$, (f) $1.5L_s$, $1.5\psi_f$.

TABLE 5. The stator current amplitude and THD value.

The type of parameter mismatch	CMPTC		IMPTC		ASPSO-IMPTC	
	Stator current	THD	Stator current	THD	Stator current	THD
$0.5L_s$	8.4137	9.86	8.4135	3.91	8.4122	3.37
$0.5\psi_f$	12.6325	9.67	12.6321	3.85	12.6311	3.25
$0.5L_s$, $0.5\psi_f$	12.6337	9.97	12.6329	4.01	12.6317	3.58
$1.5L_s$	8.4139	9.61	8.4133	3.81	8.4106	3.18
$1.5\psi_f$	5.6237	9.79	5.6225	3.83	5.6217	3.23
$1.5L_s$, $1.5\psi_f$	5.6225	9.64	5.6214	3.85	2.6209	3.29

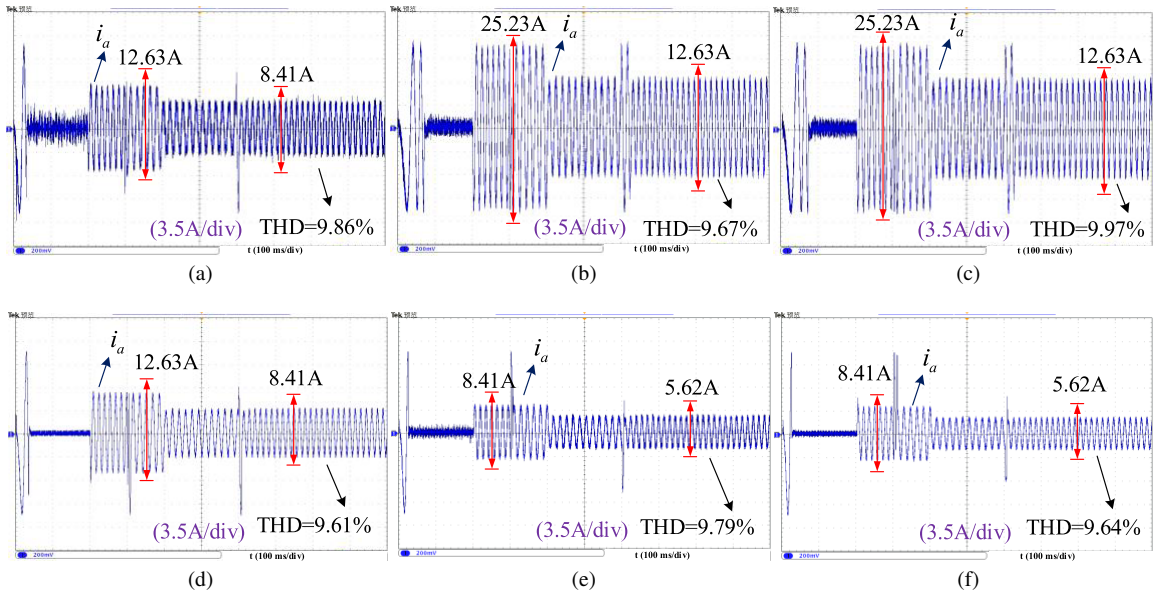

FIGURE 16. The waveform of the stator current of CMPTC with parameter mismatch. (a) $0.5L_s$, (b) $0.5\psi_f$, (c) $0.5L_s$, $0.5\psi_f$, (d) $1.5L_s$, (e) $1.5\psi_f$, (f) $1.5L_s$, $1.5\psi_f$.

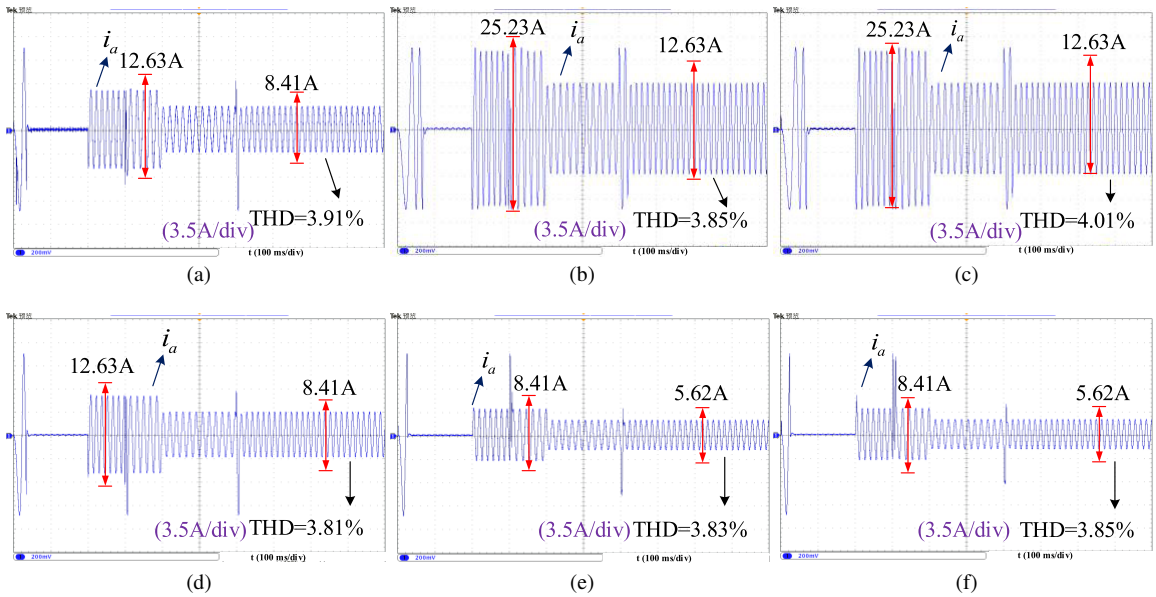

FIGURE 17. The waveform of the stator current of IMPTC with parameter mismatch. (a) $0.5L_s$, (b) $0.5\psi_f$, (c) $0.5L_s$, $0.5\psi_f$, (d) $1.5L_s$, (e) $1.5\psi_f$, (f) $1.5L_s$, $1.5\psi_f$.

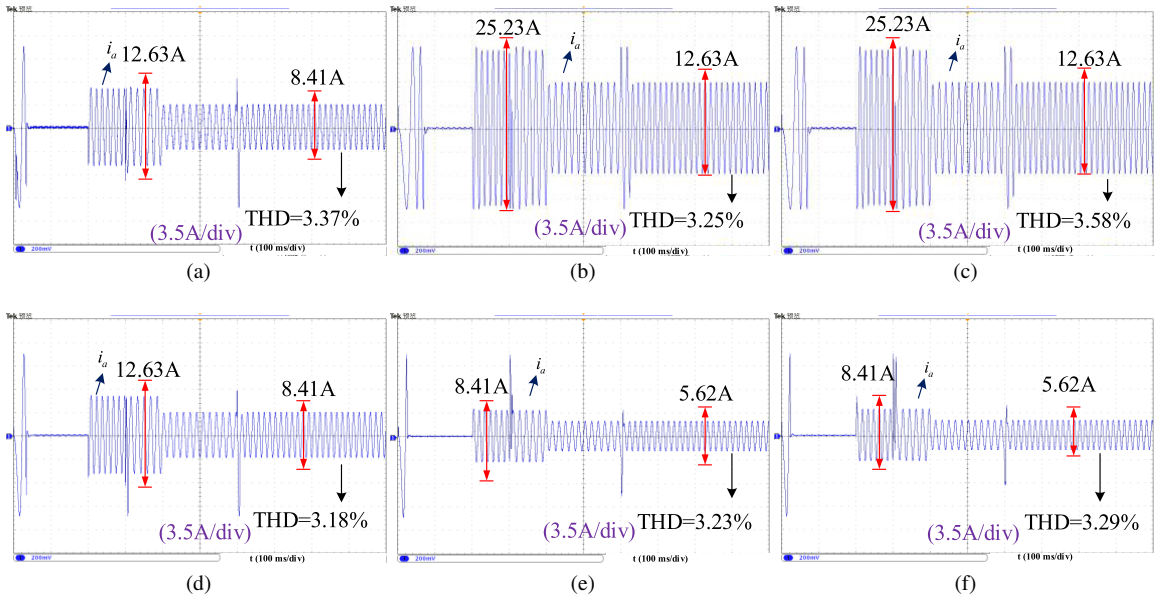

FIGURE 18. The waveform of the stator current of ASPSO-MPTC with parameter mismatch. (a) $0.5L_s$, (b) $0.5\psi_f$, (c) $0.5L_s$, $0.5\psi_f$, (d) $1.5L_s$, (e) $1.5\psi_f$, (f) $1.5L_s$, $1.5\psi_f$.

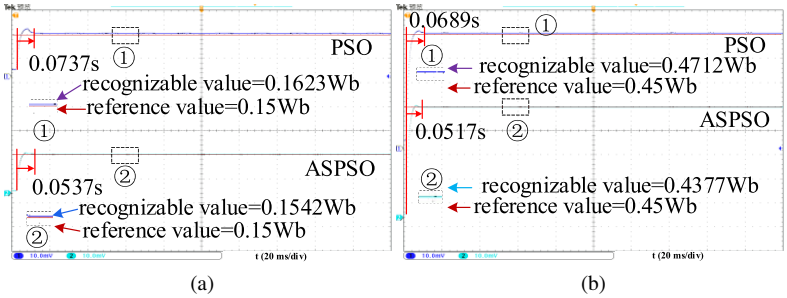

FIGURE 19. The identification diagram of the magnetic chain with parameter mismatch. (a) $0.5\psi_f$, (b) $1.5\psi_f$.

1) By comparing CMPTC and IMPTC, it can be concluded that the IMPTC strategy can still make the motor maintain a better control performance when the motor parameters are changed, while motor control performance in CMPTC is seriously deteriorated.

2) By comparing PSO-IMPTC with ASPSO-IMPTC, it can be concluded that the introduction of ASPSO makes the recognition performance of the PSO based online parameter identification algorithm further improved, and the parameter robustness of the motor is further strengthened.

5.1. The Analysis of dq-Axis Currents

Figs. 10–12 show the *dq*-axis component of PMSM current when parameter mismatch occurs under CMPTC strategy, IMPTC strategy, and ASPSO-IMPTC strategy. It can be seen that the stator current *dq*-axis component pulsation amplitude is minimized with ASPSO-IMPTC. The values of *dq*-axis current pulsation amplitude for the three strategies are shown in Table 3. Compared with IMPTC, APSO-IMPTC reduced the *d*-axis current pulsation amplitude by 38.11% and the *q*-axis current pulsation amplitude by 10.93%. Compared with CMPTC, APSO-IMPTC reduced the *d*-axis current pulsation amplitude by 85.25% and the *q*-axis current pulsation amplitude by 81.88%.

TABLE 6. The values of the magnetic chain and inductance identification.

Parameter		The identification of magnetic chain		The identification of inductors	
		$0.5\psi_f$	$1.5\psi_f$	$0.5L_s$	$1.5L_s$
PSO	Time	0.0737	0.0689	0.0586	0.0563
	Value	0.1623	0.4712	3.974	13.58
	Error	7.58%	4.50%	6.95%	6.11%
ASPSO	Time	0.0537	0.0517	0.0493	0.0486
	Value	0.1542	0.4377	4.411	13.32
	Error	2.72%	2.81%	3.65%	4.28%

5.2. The Analysis of Speed and Torque

Figs. 13–15 show the experimental waveforms of the motor speed and torque when parameter mismatch occurs under MPTC strategy, IMPTC strategy, and ASPSO-IMPTC strategy, which shows that the speed responses of the three strategies are

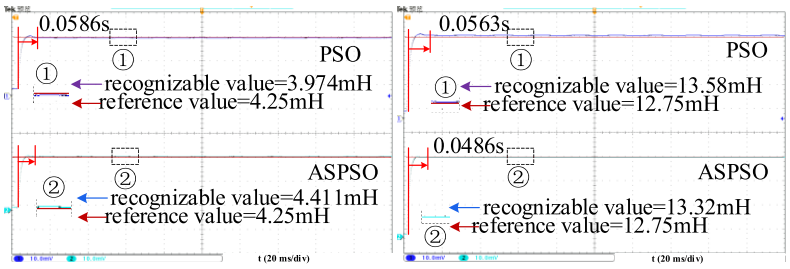

(a) (b)

FIGURE 20. The identification diagram of inductance with parameter mismatch. (a) $0.5L_s$, (b) $1.5L_s$.

TABLE 7. Comparison of PSO variants for parameter identification.

Algorithm	Improvement Strategy	Complexity	Real-Time Suitability	Real-Time Suitability
Adaptive PSO [19]	Parameter-tuning	Medium	Limited	Moderate
Hybrid PSO [20]	Algorithm fusion	High	Low	High
ASPSO (Proposed)	Review-based anti-stagnation	Low	High	High

basically the same. The speed response time and electromagnetic torque pulsation amplitude when the motor undergoes parameter mismatch are shown in Table 4. It can be seen that the electromagnetic torque under ASPSO-IMPTC has the smallest pulsation amplitude. Compared to CMPTC, ASPSO-IMPTC reduces the electromagnetic torque pulsation by 69.90%. Compared with IMPTC, the amplitude of electromagnetic torque pulsation is reduced by 8.05% in ASPSO-IMPTC.

5.3. The Analysis of Stator Currents and Harmonics

Figs. 16–18 show the stator current waveforms under the occurrence of parameter mismatch in CMPTC strategy, IMPTC strategy, and ASPSO-IMPTC strategy. It can be seen that the stator current waveform under ASPSO-IMPTC is optimal, and the total harmonic distortion (THD) value is the lowest. Table 5 shows the stator current magnitude and THD values for different strategies with parameter mismatch. Compared with CMPTC, the value of THD was reduced by 66.02% in ASPSO-IMPTC. Compared with IMPTC, the value of THD was reduced by 14.68% in ASPSO-IMPTC.

5.4. The Analysis of Parameter Identification

Figs. 19–20 show the identified waveforms of the parameters under the occurrence of parameter mismatch in PSO strategy and the proposed strategy ASPSO. The figure also reflects the convergence speed and steady-state accuracy of the identification process. The recognition time and recognition error are shown in Table 6. The ASPSO identifies the inductance with an error of 3.97% and an identification time of 0.04895 s, and recognizes the magnetic chain with an error of 2.77% and an identification time of 0.05270 s. Compared to PSO, the magnetic chain identification error is reduced by 54.14%, and the identification time is reduced by 31.35%. The recognition error of the inductor is reduced by 39.20%, and the recognition time is reduced by 14.80%.

Table 7 compares the proposed ASPSO algorithm with common PSO variants. Unlike adaptive or hybrid PSO approaches, which increase algorithmic complexity through parameter tuning or integration with other heuristics, ASPSO introduces a lightweight review mechanism that effectively prevents swarm stagnation. This allows for improved robustness and identification accuracy without compromising real-time performance, making it highly suitable for online parameter estimation in PMSM drives.

6. CONCLUSION

To address the problem that the control performance of the motor in the conventional MPTC (CMPTC) strategy is heavily dependent on the motor parameters, an improved model predictive torque control (IMPTC) for PMSM based on anti-stagnation particle swarm online parameter identification (ASPSO-IMPTC) is proposed. The following can be concluded from the analysis of theoretical studies and experimental results:

1) The proposed IMPTC strategy uses the motor parameters after parameter extraction compensation instead of the motor parameters at parameter mismatch. Compared with CMPTC strategy, the d-axis current pulsation value is reduced by 76.17%, q-axis current pulsation value reduced by 79.66%, torque pulsation value reduced by 67.26%, and stator current THD reduced by 60.19%.

2) The proposed ASPSO-IMPTC strategy incorporates a monitoring mechanism into the particle swarm optimization (PSO) identification process. This innovation effectively prevents particle stagnation and significantly enhances PSO' motor parameter identification accuracy. Compared with the PSO parameter identification, the ASPSO parameter identification reduces the inductor identification error and identification time by 38.72% and 14.78%, respectively, and the magnetic chain identification error and identification time by 50.84% and 26.05%, respectively. Compared to the CMPTC strategy, the proposed ASPSO-IMPTC strategy reduces the d-axis current pulsation value by 85.25%, the q-axis current pulsation value

by 81.88%, the torque pulsation value by 69.90%, and the stator current THD by 66.02%.

3) The proposed ASPSO-IMPTC strategy not only improves the accuracy and convergence speed of online parameter identification, but also enhances the robustness of motor control under parameter mismatch and dynamic operating conditions. Due to its lightweight structure and real-time performance, the method is well suited for practical industrial applications that require reliable and adaptive motor drive control. Potential application areas include electric vehicles, aerospace actuators, and high-performance servo systems, where precise torque control and parameter tracking are critical for system safety and efficiency.

ACKNOWLEDGMENT

This work was supported by the Scientific Research Fund of Hunan Provincial Education Department under Grant Number 24A0395.

REFERENCES

[1] Zhu, L., B. Xu, and H. Zhu, "Interior permanent magnet synchronous motor dead-time compensation combined with extended Kalman and neural network bandpass filter," *Progress In Electromagnetics Research M*, Vol. 98, 193–203, 2020.

[2] Zhang, Y., S. Li, B. Luo, C. Luo, and Z. Yu, "Output current harmonic analysis and suppression method for PMSM drive system with modular multilevel converter," *IET Renewable Power Generation*, Vol. 17, No. 13, 3289–3297, Oct. 2023.

[3] Zhang, H., T. Fan, L. Meng, *et al.*, "Polynomial estimation of chain for predictive current control in PMSM," *IEEE Journal of Emerging and Selected Topics in Power Electronics*, Vol. 10, No. 5, 6112–6122, Oct. 2022.

[4] Liu, X., Y. Pan, L. Wang, J. Xu, Y. Zhu, and Z. Li, "Model predictive control of permanent magnet synchronous motor based on parameter identification and dead time compensation," *Progress In Electromagnetics Research C*, Vol. 120, 253–263, 2022.

[5] Liu, X., Y. Pan, Y. Zhu, H. Han, and L. Ji, "Decoupling control of permanent magnet synchronous motor based on parameter identification of fuzzy least square method," *Progress In Electromagnetics Research M*, Vol. 103, 49–60, 2021.

[6] Wang, Y., Y. Xu, and J. Zou, "Online multiparameter identification method for sensorless control of SPMSM," *IEEE Transactions on Power Electronics*, Vol. 35, No. 10, 10 601–10 613, Oct. 2020.

[7] Cheng, Z., C. Zhang, and Y. Zhang, "PMSWG parameter identification method based on improved operator genetic algorithm," *Progress In Electromagnetics Research C*, Vol. 139, 67–77, 2023.

[8] Yuan, X., S. Zhang, and C. Zhang, "Improved model predictive current control for SPMSM drives with parameter mismatch," *IEEE Transactions on Industrial Electronics*, Vol. 67, No. 2, 852–862, Feb. 2020.

[9] Yan, L., M. Dou, Z. Hua, H. Zhang, and J. Yang, "Robustness improvement of FCS-MPTC for induction machine drives using disturbance feedforward compensation technique," *IEEE Transactions on Power Electronics*, Vol. 34, No. 3, 2874–2886, Mar. 2019.

[10] Zhang, X., C. Zhang, Z. Wang, and J. Rodríguez, "Motor-parameter-free model predictive current control for PMSM drives," *IEEE Transactions on Industrial Electronics*, Vol. 71, No. 6, 5443–5452, Jun. 2024.

[11] Zhang, Y., Z. Yin, W. Li, J. Liu, and Y. Zhang, "Adaptive sliding-mode-based speed control in finite control set model predictive torque control for induction motors," *IEEE Transactions on Power Electronics*, Vol. 36, No. 7, 8076–8087, Jul. 2021.

[12] Zhang, X., Z. Wang, Z. Zhao, and M. Cheng, "Model predictive voltage control for SPMSM drives with parameter robustness optimization," *IEEE Transactions on Transportation Electrification*, Vol. 8, No. 3, 3151–3163, Sep. 2022.

[13] Li, X. and R. Kennel, "General formulation of Kalman-filter-based online parameter identification methods for VSI-fed PMSM," *IEEE Transactions on Industrial Electronics*, Vol. 68, No. 4, 2856–2864, Apr. 2021.

[14] Wang, L., S. Zhang, C. Zhang, and Y. Zhou, "An improved deadbeat predictive current control based on parameter identification for PMSM," *IEEE Transactions on Transportation Electrification*, Vol. 10, No. 2, 2740–2753, Jun. 2024.

[15] Wang, Q., G. Wang, N. Zhao, G. Zhang, Q. Cui, and D. Xu, "An impedance model-based multiparameter identification method of PMSM for both offline and online conditions," *IEEE Transactions on Power Electronics*, Vol. 36, No. 1, 727–738, Jan. 2021.

[16] Wang, Z., J. Chai, X. Xiang, X. Sun, and H. Lu, "A novel online parameter identification algorithm designed for deadbeat current control of the permanent-magnet synchronous motor," *IEEE Transactions on Industry Applications*, Vol. 58, No. 2, 2029–2041, Mar.-Apr. 2022.

[17] Xie, C., S. Zhang, X. Li, Y. Zhou, and Y. Dong, "Parameter identification for SPMSM with deadbeat predictive current control using online PSO," *IEEE Transactions on Transportation Electrification*, Vol. 10, No. 2, 4055–4064, Jun. 2024.

[18] Liu, Z.-H., H.-L. Wei, X.-H. Li, K. Liu, and Q.-C. Zhong, "Global identification of electrical and mechanical parameters in PMSM drive based on dynamic self-learning PSO," *IEEE Transactions on Power Electronics*, Vol. 33, No. 12, 10 858–10 871, Dec. 2018.

[19] Sandre-Hernandez, O., R. Morales-Caporal, J. Rangel-Magdaleno, H. Peregrina-Barreto, and J. N. Hernandez-Perez, "Parameter identification of PMSMs using experimental measurements and a PSO algorithm," *IEEE Transactions on Instrumentation and Measurement*, Vol. 64, No. 8, 2146–2154, Aug. 2015.

[20] Zhang, Y., M. Zhou, C. Zhang, A. Shen, and L. Bing, "Identification of PMSM parameters with time-error compensated based on contractile factor antipredator PSO," *IEEE Transactions on Transportation Electrification*, Vol. 10, No. 2, 4006–4017, Jun. 2024.

[21] Bekhouche, L., R. Saou, C. Guerroudj, A. Kouzou, and M. E.-H. Zaim, "Electromagnetic torque ripple minimization of slotted doubly-salient-permanent-magnet generator for wind turbine applications," *Progress In Electromagnetics Research M*, Vol. 83, 181–190, 2019.

[22] Kendjouh, T., C. Guerroudj, J.-F. Charpentier, N. Bracikowski, L. Hadjout, and L. Bekhouche, "Contribution to improve magnetic performance and torque ripple reduction of the low-speed DSPM machine," in *Actuators*, Vol. 12, No. 5, 195, 2023.

[23] Zhang, Y., C. Zhang, and Z. Cheng, "Parameter identification based on chaotic map simulated annealing genetic algorithm for PMSWG," *Progress In Electromagnetics Research M*, Vol. 113, 59–71, 2022.

[24] Liu, K. and Z. Q. Zhu, "Position-offset-based parameter estimation using the adaline NN for condition monitoring of permanent-magnet synchronous machines," *IEEE Transactions on Indus-*

trial Electronics, Vol. 62, No. 4, 2372–2383, Apr. 2015.

[25] Niedermayr, P., L. Alberti, S. Bolognani, and R. Abl, "Implementation and experimental validation of ultrahigh-speed PMSM sensorless control by means of extended Kalman filter," *IEEE Journal of Emerging and Selected Topics in Power Electronics*, Vol. 10, No. 3, 3337–3344, Jun. 2022.

[26] Zhang, X., Y. Cao, C. Zhang, and S. Niu, "Model predictive control for PMSM based on the elimination of current prediction errors," *IEEE Journal of Emerging and Selected Topics in Power Electronics*, Vol. 12, No. 3, 2651–2660, Jun. 2024.